coatings

MDPI

Article

Tribological Properties of Laser-Cladded NiCrBSi Coatings Undergoing Friction with Ti6Al4V Alloys

Mingzhen Fan, Pengcheng Du, Ke Wen, Ruizhi Zhang, Siliang Yu and Tongzhou Chen *

State Key Laboratory of Special Surface Protection Materials and Application Technology, China Academy of Machinery, Wuhan Research Institute of Materials Protection Co., Ltd., Wuhan 430030, China; fanmingzhen0423@126.com (M.F.); lydpch@163.com (P.D.); wk13545197613@163.com (K.W.); 13477086535@163.com (R.Z.); yusiliang110@163.com (S.Y.)

* Correspondence: chentongzhou@rimp.com.cn

Abstract: This work aims at reducing abrasion between titanium alloy parts, such as drive shafts and support pairs used in aviation. Three different NiCrBSi coatings, Ni40, Ni50, and Ni60, are prepared on surfaces of Ti6Al4V by laser cladding. The microstructural and mechanical properties of these coatings are analyzed by scanning electron microscope (SEM) and a microhardness tester. The tribological properties of the NiCrBSi coatings undergoing friction with Ti6Al4V are tested using a wear testing machine. The results show that the Vickers hardnesses of the Ni40, Ni50, and Ni60 coatings are 490 $HV_{0.3}$, 609 $HV_{0.3}$, and 708 $HV_{0.3}$, respectively. For the above NiCrBSi coatings, more hard phases are produced with increases in the amounts of Cr in the powders, resulting in increases in the coatings' hardnesses. The wear test results show that the NiCrBSi coatings could reduce the friction coefficients, which gradually decreased with increases in the coatings' hardnesses. Both the coating-specific wear rates and the friction pair wear losses initially decreased and then increased. The Ni50 coating and the Ti6Al4V friction pair undergoing friction with the Ni50 coating showed the best wear performance, with a specific wear rate and wear loss of 0.51 × 10^{-7} $mm^3/(N{\cdot}m)$ and 7.8 mg, respectively. The specific wear rates for Ni50 were only 8.4%, 35.4%, and 37.0% of the Ti6Al4V, Ni40, and Ni60, respectively. In addition, the friction pair wear loss was only 36.4%, 52.5%, and 55.3% of that while undergoing friction with Ti6Al4V, Ni40, and Ni60, respectively. The NiCrBSi coatings prepared on the surface of Ti6Al4V show excellent antifriction and wear resistance properties, providing a viable solution for the design of wear-resistant coatings on load-bearing and non-load-bearing titanium alloy parts.

Keywords: laser cladding; Ti6Al4V alloy; NiCrBSi coating; hardness; tribological properties

check for updates

Citation: Fan, M.; Du, P.; Wen, K.; Zhang, R.; Yu, S.; Chen, T. Tribological Properties of Laser-Cladded NiCrBSi Coatings Undergoing Friction with Ti6Al4V Alloys. *Coatings* **2024**, *14*, 813. https://doi.org/10.3390/coatings14070813

Academic Editor: Rafael Comesaña

Received: 9 May 2024
Revised: 14 June 2024
Accepted: 21 June 2024
Published: 28 June 2024

Copyright: © 2024 by the authors. Licensee MDPI, Basel, Switzerland. This article is an open access article distributed under the terms and conditions of the Creative Commons Attribution (CC BY) license (https://creativecommons.org/licenses/by/4.0/).

1. Introduction

Ti6Al4V is extensively employed in aviation equipment, such as aircraft flap slides and engine-bearing seats, owing to its high specific strength and exceptional corrosion resistance [1–4]. However, the Ti6Al4V alloy undergoes significant wear loss due to its low hardness [5] and thermal conductivity [6] and poor resistance to adhesive wear [7]. The strong adhesion and low shear resistance that result in serious wear of the titanium alloy in the case of friction between the titanium alloy parts [8]. To enhance the wear performance of titanium alloys, researchers have developed coatings such as NiCr BSi [9–12], TiC/TiAl [13–15], and CuNiIn [15,16] through laser cladding and high-velocity oxygen fuel. Nevertheless, surface protective coatings typically diminish the fatigue life of components [15,17]. Therefore, for load-bearing and non-load-bearing Ti alloy component systems in aviation, designing a protective coating for non-load-bearing titanium alloy surfaces to reduce wear while maintaining the fatigue strength of load-bearing Ti alloy parts is crucial research with industrial application value.

The CuNiIn coating demonstrates excellent fretting wear resistance on titanium alloy, which is widely used in conditions of Ti/Ti alloy contact [15,16,18]. However, the CuNiIn coating experiences significant wear under high contact loads and large sliding distances due to its low hardness [18]. In such cases, coatings with higher hardness, shear resistance, and self-lubrication properties can reduce the level of abrasion [19,20]. NiCrBSi has a low melting point (993 °C) [21], good wettability with titanium alloy [22], moderate hardness (HRC30~60), and a thermal expansion coefficient (1.14×10^{-5}/K) that is compatible with Ti6Al4V alloy substrates [22], making it an ideal material for wear-resistant coatings on titanium alloy surfaces. The results in Reference [19] indicate that a lower combined wear loss was obtained when the Ni45 coating underwent friction with the Ti6Al4V friction pair. However, the low fracture toughness of thermally sprayed NiCrBSi coatings easily causes spraying particles to peel off under larger contact loads [19]. Therefore, laser cladding—a coating preparation process that can improve microstructures and enhance toughness—is used to prepare NiCrBSi coatings on titanium alloy surfaces [10,23,24]. The laser-cladded NiCrBSi coating forms good metallurgical bonds with Ti6Al4V substrates. The hardness of NiCrBSi coatings is about 1000 HV, showing an improvement in the wear resistance by about 10 times that of the substrate [23]. Li et al. [24] prepared NiCrBSi coatings on Ti6Al4V by laser cladding. NiCrBSi coatings show excellent wettability with Ti6Al4V alloy, as well as a more notable wear resistance than the substrate. Furthermore, hard phases such as TiN, TiC, B_4C, and WC [10,11,25–27], as well as the lubrication phases h-BN [10,22] and WS_2 [22,28], are utilized to enhance the wear resistance of NiCrBSi coatings. In previous studies, the wear resistances of NiCrBSi coatings were characterized by Si_3N_4 or Gr15 friction pairs. However, the friction match between NiCrBSi coatings and titanium alloys was not studied.

In this work, three NiCrBSi coatings with different hardnesses were prepared on the surfaces of Ti6Al4V by laser cladding, and the wear performances of the coatings undergoing friction with Ti6Al4V were studied as well. The best suitable mechanical properties of the coatings that reduce the amount of comprehensive wear of the coating and Ti6Al4V friction pair were obtained, which provide technical support in the design of wear-resistant coatings for load-bearing and non-load-bearing titanium alloy parts.

2. Experimental Materials and Procedures

2.1. Experimental Materials and Coating Preparation

A $70 \times 50 \times 10$ mm^3 Ti6Al4V plate was used as the substrate to prepare the NiCrBSi coatings. The oxide layer of the substrate was removed by grinding with sandpaper and cleaned with acetone before the laser cladding. Three different NiCrBSi powders (ZhuJin Technology Co., Ltd., Tianjin, China), named Ni40, Ni50, and Ni60, respectively, with sizes of 15–53 μm, were used as feedstock materials. The chemical compositions of the NiCrBSi powders are shown in Table 1. An YLS-2000 laser cladding system (IPG Photonics, Oxford, MA, USA) was used to prepare the NiCrBSi coatings, and Ar was used as a protection gas with a gas flow rate of 18–20 L/min. The laser power was 2 kW, with a scanning speed of 4 mm/s and a spot diameter of 4 mm, respectively. The appearances of the laser-cladded NiCrBSi coatings are shown in Figure 1.

Table 1. Chemical compositions of the powders (wt%).

Element	C	Cr	Si	Fe	B	Ni
Ni40	0.30	7.50	3.0	≤8.0	1.7	Bal.
Ni50	0.45	11.0	4.0	≤8.0	2.2	Bal.
Ni60	0.70	15.0	4.0	≤8.0	3.2	Bal.

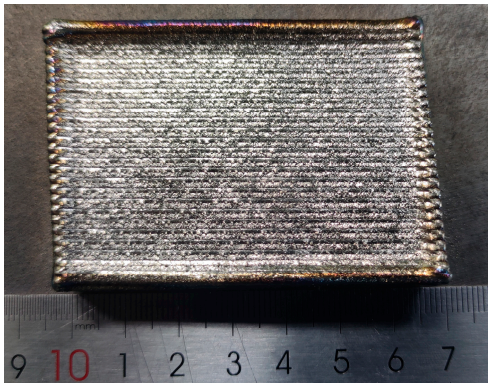


Figure 1. The appearance of a laser-cladded NiCrBSi coating.

2.2. Microstructure Characterization and Microhardness Tests

The cladded NiCrBSi layer was cut into dimensions of 10 × 10 × 3 mm^3 by using electrical discharge wire cutting, and then the cross-sections of the specimens were ground and polished for microstructure characterization and the microhardness test. The cross-section microstructure of the coatings was observed by using a JSM-6510LV scanning electron microscope (JEOL, Tokyo, Japan). The coating phase structure was analyzed on a SmartLab SE intelligent multifunctional X-ray diffractometer (Rigaku, Kyoto, Japan). The microhardness of the coatings was measured using a WHV-1000AMT Vickers hardness tester at a load of 2.94 N with a dwelling time of 15 s, and each value was averaged over 10 measurements.

2.3. Wear Tests

The tribological properties of the coatings in friction with Ti6Al4V were tested 5 times on an MXW-1 multifunctional tribometer (Jinan Yihua Tribological Testing Technology Co., Ltd., Jinan, China). All the coatings and the friction pairs were ground and polished to a surface roughness of R_z 0.8–1.5 μm before testing. The friction test scheme is shown in Figure 2, in which the diameter of the Ti6Al4V friction pair is 4.8 mm. The Ti6Al4V friction pair and coatings formed plane/plane contact at a load of 100 N, and the friction process lasted for 60 min with a sliding distance of 8 mm at a frequency of 5 Hz.

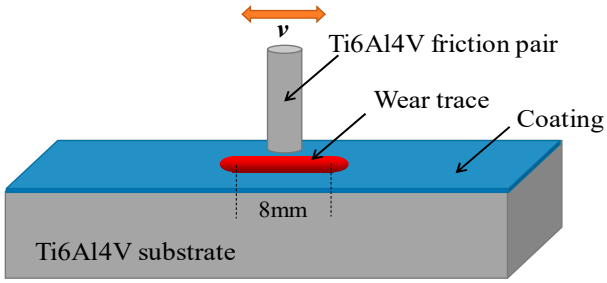


Figure 2. Friction test scheme.

The wear trace morphology of both coatings and friction pairs were observed by using a JSM-6510LV scanning electron microscope. The morphology and depth of the coating wear trace were analyzed by a white light confocal three-dimensional morphology tester (Sciences et Techniques Industrielles de la Lumière, Aix-en-Province, France). A mitutoyo SJ-210 surface roughness tester (Mitutoyo, Kanagawa, Japan) was used to measure the wear trace roughness of the coatings and Ti6Al4V friction pairs, in which the test direction was perpendicular to the direction of friction motion. The coating-specific wear rate was obtained by Equation (1), in which the volume of wear trace was integrated via Origin

software. The wear losses of the Ti6Al4V friction pairs were weighed by an electronic balance with a sensitivity of 10^{-4} g (Jingke, Shanghai, China).

$$\omega = \frac{V}{f \times s \times t \times F} \quad (1)$$

where V is the wear volume, f the sliding frequency, t the test time, s the sliding distance for one trace, and F the pressure load.

3. Results and Discussion

3.1. Coating Composition and Phase Structure

Figure 3 depicts the XRD patterns of the NiCrBSi powders and coatings. The XRD data were normalized by the intensity of the diffraction peak at 2θ = 44° from the γ-(Fe, Cr, Ni) phase. It is evident from the data that the three NiCrBSi powders are primarily composed of the γ-(Fe, Cr, Ni) phase and other hard phases such as Cr-C and Cr-B [29,30]. The diffraction peak intensities of the Cr-C and Cr-B phases show no significant differences among the three NiCrBSi powders. However, the diffraction peak intensity of the γ-(Fe,Cr,Ni) phase in the three NiCrBSi coatings is significantly enhanced after laser cladding, while there is only a slight enhancement in the intensity of the $Cr_{23}C_6$ and CrB phase diffraction peaks compared to the powders. Notably, both the Ni50 and Ni60 coatings exhibit significantly higher diffraction intensities of the $Cr_{23}C_6$, Cr_7C_3, and CrB phases than the Ni40 coatings. This can be attributed to a high energy input from the laser that promotes the formation of ceramic hard phases such as $Cr_{23}C_6$ and Cr_7C_3 [29–31]. Meanwhile, as indicated in Table 1, both the Ni50 and Ni60 powders contain higher amounts of C and Cr than Ni40 powders, which results in forming more Cr-C and Cr-B phases. As shown in Figure 3c, the (Fe,Cr,Ni)C phase is detected in the Ni60 coating. It can be inferred that the C has a solid solution with the γ-(Fe,Cr,Ni) phase and results in the Fe,Cr,Ni)C phase.

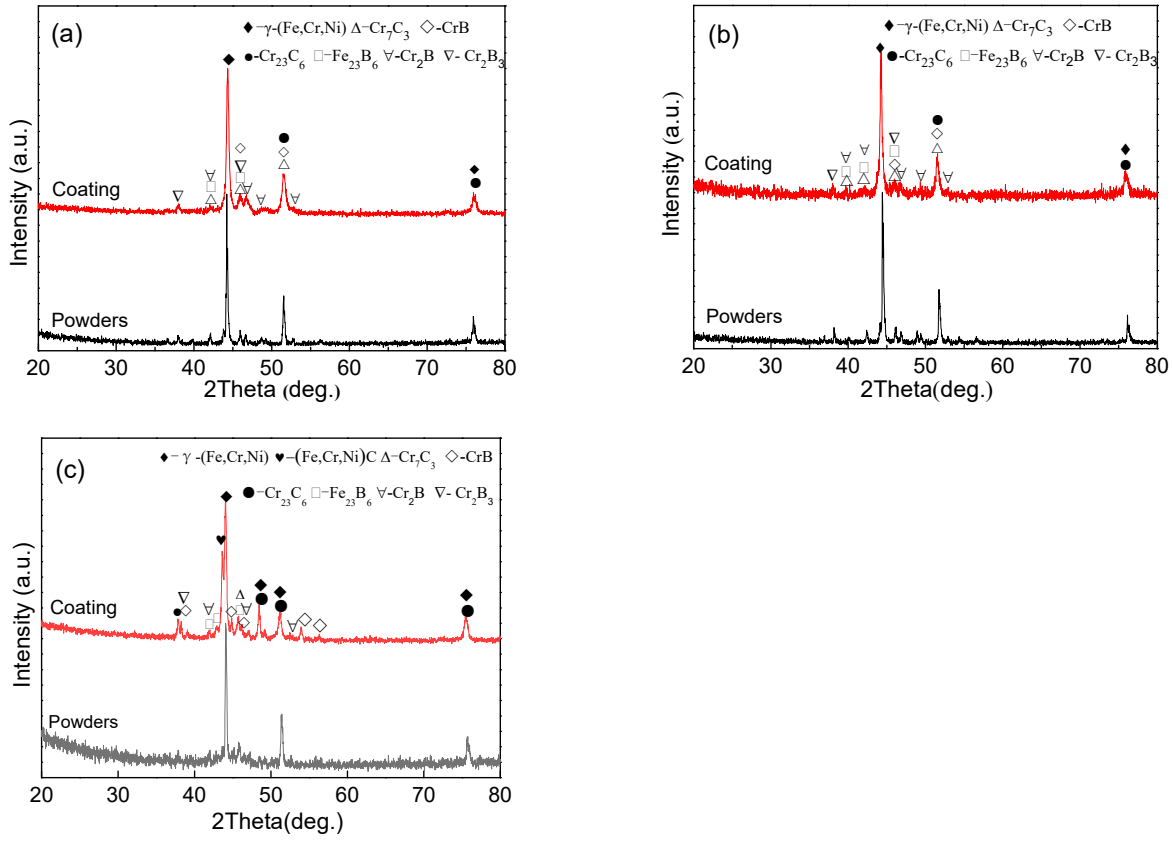


Figure 3. XRD patterns of the powders and laser cladding coatings: (**a**) Ni40; (**b**) Ni50; (**c**) Ni60.

3.2. Coating Microstructure and Mechanical Properties

Figure 4 shows the metallograph of the coating. All the NiCrBSi coatings are dense and poreless, and form metallurgical bonding with the Ti6Al4V substrate. The Ni40 coating shows a dendritic structure (Figure 3a,b) that grows perpendicular from the bottom to the top surface. The coating structure is the same as the NiCrBSi coating in ref [29]. The dendritic structure is considered to be γ-Ni [32]. The Ni50 coating (Figure 4c,d) shows a dendritic structure with several granular precipitates. Furthermore, the size of the granular precipitates in the Ni60 coating (Figure 4e,f) enlarged, and the dendritic structure is discontinuous. The chemical compositions of Ni40 and Ni60 are the same as the NiCrBSi coatings in Ref. [29]; the same metallographic as those in Ref. [29] are also observed in this study.

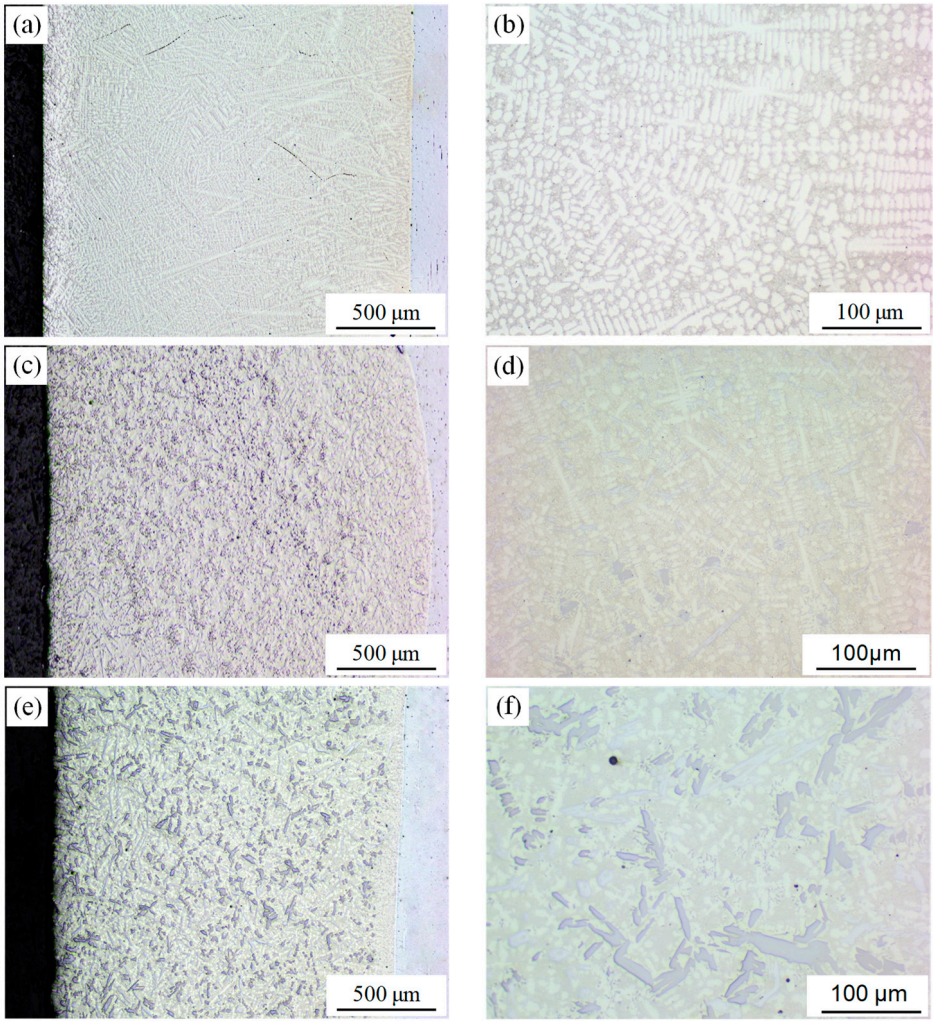


Figure 4. Metallograph of the coating: (**a**,**b**) Ni40; (**c**,**d**) Ni50; (**e**,**f**) Ni60.

The SEM images in Figure 5, Figure 6, and Figure 7 display the Ni40, Ni50, and Ni60 coatings, respectively, along with the distribution of Ni, Cr, C, and B, which was determined by mapping analysis. The SEM images are taken from the middle of the coatings, as shown in Figure 4. In Figure 5, small grain particles ranging from 10 to 20 μm are observed within the Ni40 coatings. The distribution of these grains correlates well with that of the Cr element; similarly, the distribution of Cr aligns closely with that of the C and B elements. On the basis of the XRD analysis and element mapping results, it can be inferred that these grain particles consist of Cr-C and Cr-B hard phases.

The metallographic structure of Ni50 coating is depicted in Figure 6, showing an increase in the grain size of Cr-C and Cr-B hard phases to 50–100 μm. Additionally, several

dispersively distributed Cr phases with a size of 20–30 μm can still be observed within the coating. In Figure 6, as the chromium content in the coating increases, the dispersed Cr-C phase undergoes a transition from a hard phase to a granular Cr-C phase. Meanwhile, the grain size of the Cr-C and Cr-B hard phases further grows to a size of 100 μm. Houdková et al. [33] reported that the metallographic structure of the NiCrBSi coating, which has a similar elemental composition to Ni60, exhibits irregular blocky and needle-like particles resembling those observed in the Ni60 coating; these blocky particles are typically identified as the M_6C hard phase [34]. The morphology of hard phase particles in both Ni50 and Ni60 coatings demonstrates distinct nonuniform nucleation characteristics due to higher contents of elements favoring the formation of hard phases (such as C and Cr) as well as smaller critical nucleation sizes for nonuniform nucleation compared to uniform nucleation [35], resulting in the formation of irregularly shaped hard phase particles.

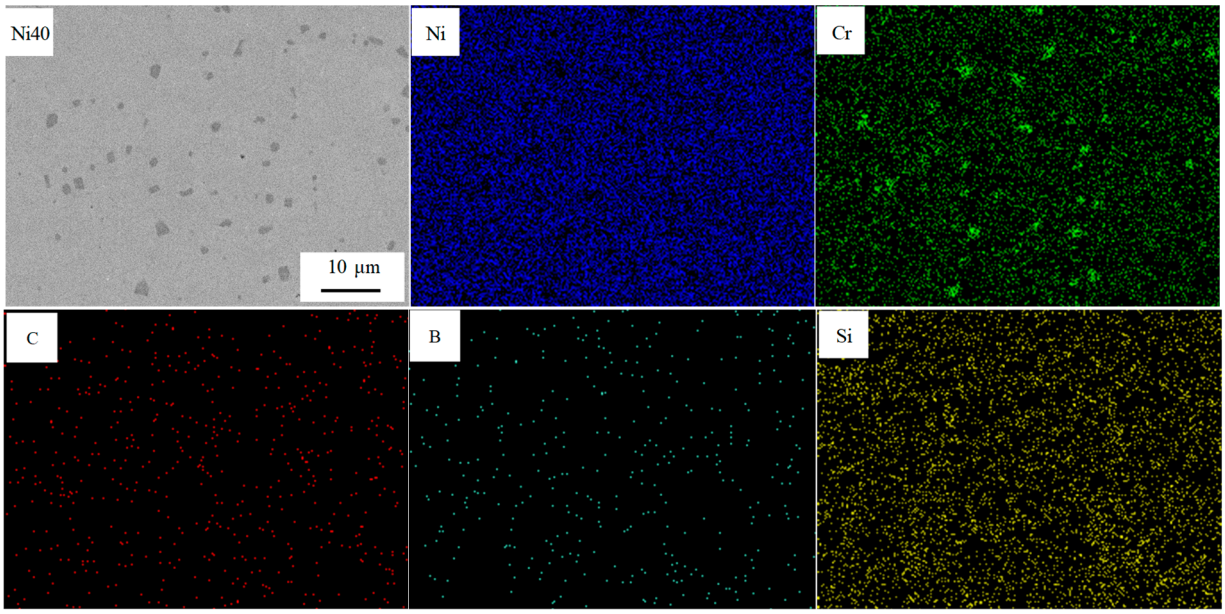


Figure 5. SEM image of the Ni40 coatings.

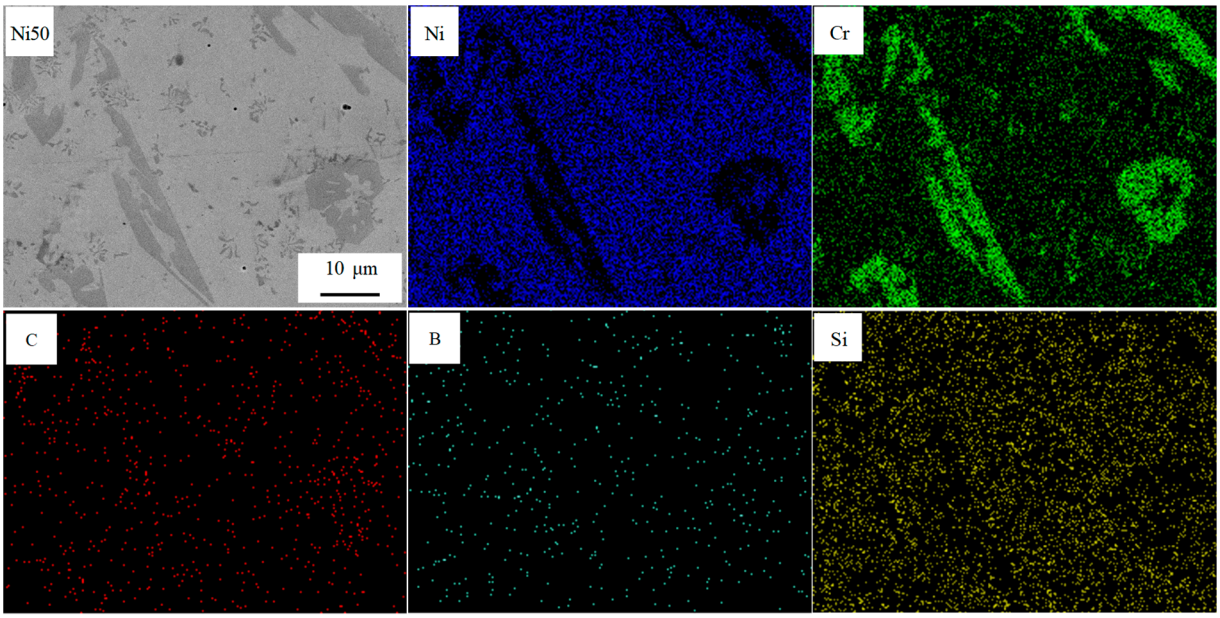


Figure 6. SEM image of the Ni50 coatings.

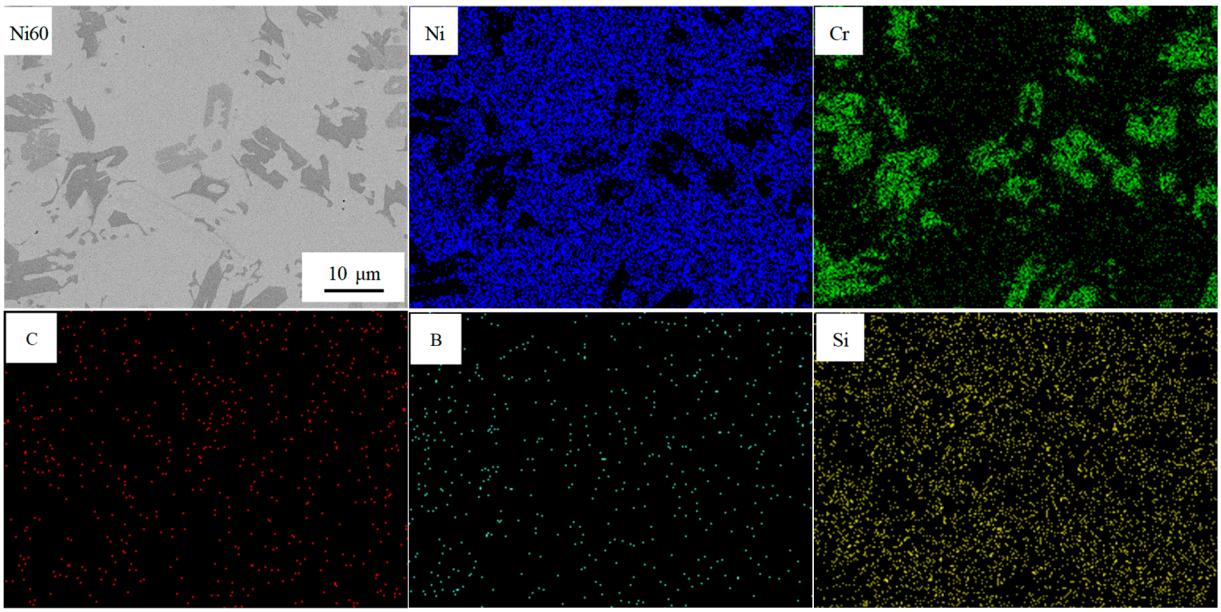


Figure 7. SEM image of the Ni60 coatings.

The microhardness of the Ti6Al4V substrate and the three NiCrBSi coatings is presented in Figure 8. The microhardness of the Ti6Al4V is approximately 314 $HV_{0.3}$, whereas the microhardness values for the Ni40, Ni50, and Ni60 coatings are 490 $HV_{0.3}$, 609 $HV_{0.3}$, and 708 $HV_{0.3}$, respectively. The gradual increase in Fe, Cr, C, and B content in the Ni40, Ni50, and Ni60 coatings as shown in Table 1 promotes the formation of hard phases such as Cr-C and Cr-B during the laser cladding process. Additionally, SEM images indicate that the sizes of hard phase particles in the Ni50 and Ni60 coatings are significantly larger than those in the Ni40 coating due to an increased content of ceramic hard phases (e.g., $Cr_{23}C_6$, Cr_7C_3, CrB, and Cr_2B_3), resulting in enhanced coating hardness [23,24].

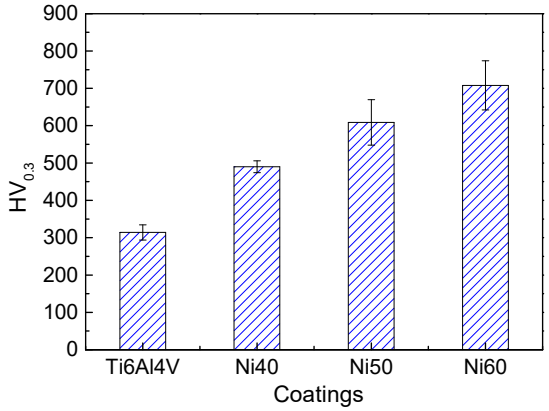


Figure 8. The microhardness of the coatings and Ti6Al4V substrate.

3.3. Tribological Properties of the Coatings

The friction coefficient curves of the coatings that are in friction with the Ti6Al4V friction pair are depicted in Figure 9. The initial 100 s of the friction process represent the running-in stage between the coating and the friction pair, during which there is significant fluctuation in the friction coefficient. After 100 s of sliding, the surface of both the friction pair and coating are fully mated, resulting in a relatively stable friction coefficient. The maximum friction coefficient occurs between the Ti6Al4V substrate and its corresponding friction pair, reaching approximately 0.71. The friction coefficient of Ti6Al4V that is in friction with 316L ranges from 0.4 to 0.9 with a load of 100N, indicating

a high friction coefficient of the friction between Ti6Al4V and metals due to the effect of plastic deformation and adhesion [36]. Since the titanium alloys show poor adhesive wear resistance [7], it seems plausible that the friction between titanium alloys achieves a high friction coefficient due to deformation and adhesion. With increasing coating hardness, the friction coefficients between the Ti6Al4V friction pair and Ni40, Ni50, and Ni60 coatings gradually decrease to 0.69, 0.62, and 0.57, respectively, indicating that these coefficients are lower than those between Ti6Al4V and its corresponding friction pair. Within a narrow time interval during sliding, a slight fluctuation in the friction coefficient is observed. Similar fluctuation patterns are also noted in previous studies on wear tests when the WC-Ni, Ni45, and NiCr coatings are in friction with Ti6Al4V [19].

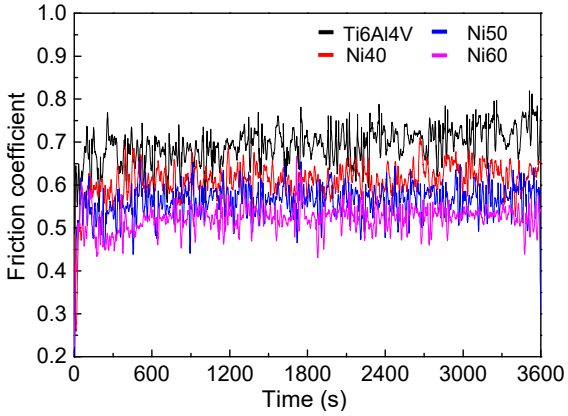


Figure 9. The friction coefficient of different NiCrBSi coatings in friction with Ti6Al4V.

The cross-section wear profiles of the coatings obtained by the white light confocal microscopy are presented in Figure 10. The maximum wear depth is observed in the friction between Ti6Al4V alloys, reaching a peak value of approximately 290 μm. However, the wear depth of the coatings does not exhibit a gradual decrease with increasing coating hardness. Specifically, the Ni50 coating demonstrates the lowest wear depth at about 26 μm, significantly lower than both the Ni40 and Ni50 coatings, which have wear depths of 78 μm and 75 μm, respectively.

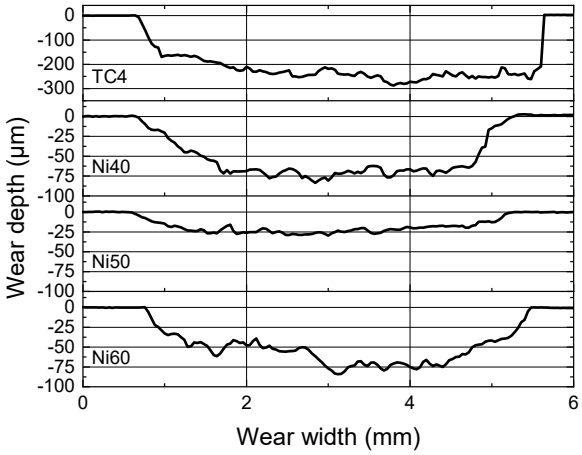


Figure 10. The wear profile of Ti6Al4V and NiCrBSi coatings.

The wear trace surface roughness *Rz* of the NiCrBSi coatings and Ti6Al4V friction pair are presented in Figure 11. The surface roughness of the Ti6Al4V substrate is approximately 22.1 μm, which is similar to that of the friction pair at 22.5 μm due to their identical material composition. The wear trace roughness values for the Ni40, Ni50, and Ni60 coatings are 18.8 μm, 10.2 μm, and 10.4 μm, respectively, while those for the corresponding Ti6Al4V

friction pairs are measured at 19.8 μm, 13.5 μm, and 14.8 μm, respectively. The Ni50 coating and the Ti6Al4V friction pair demonstrate the lowest wear trace roughness, while the Ni60 coating and its corresponding friction pair exhibit lower wear trace roughness compared to the Ni40 coating. Furthermore, Figure 8 illustrates that an increase in hardness difference between the coating and its Ti6Al4V friction pair is associated with an enlargement of wear trace roughness values.

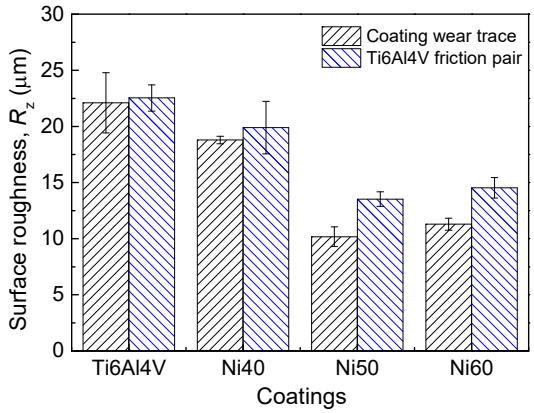


Figure 11. The wear trace roughness of NiCrBSi coatings and Ti6Al4V friction pair.

Figure 12 illustrates the coating-specific wear rate and Ti6Al4V friction pair wear loss, respectively. The specific wear rate of the coatings is calculated by Equation (1), in which the wear volume is integrated by Origin software. The specific wear rates of Ti6Al4V alloy, Ni40, Ni50, and Ni60 coatings are 6.1, 1.4, 0.5, and 1.38 × 10^{-7} $mm^3/(N{\cdot}m)$, respectively. The NiCrBSi coatings exhibit superior lubricity and higher hardness compared to the Ti6Al4V substrate, resulting in improved wear resistance. The wear loss of the Ti6Al4V friction pair measures 21.4 mg, 14.9 mg, 7.8 mg, and 14.1 mg for different coatings. Therefore, it can be concluded that the application of the NiCrBSi coating on Ti6Al4V not only enhances substrate wear performance but also reduces the wear loss of the Ti6Al4V friction pair significantly.

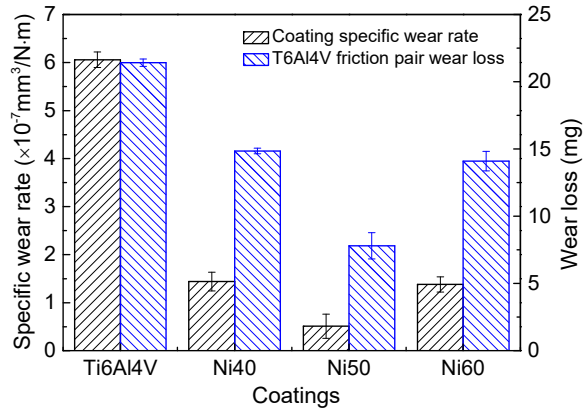


Figure 12. Coating-specific wear rate and friction pair weight loss.

3.4. Wear Trace Morphology and Wear Mechanisms

Figure 13 depicts the wear trace morphology of the NiCrBSi coatings and the Ti6Al4V friction pair. It is evident from Figure 13a that the wear trace morphology of the Ti6Al4V substrate exhibits pronounced cutting and shearing delamination features, which is the same as previous studies on Ti6Al4V wear performance [37–39]. The wear trace morphology of the Ti6Al4V friction pair, as shown in Figure 13b, displays a similar irregular undulating feature. Despite being polished before the wear test, both the Ti6Al4V substrate and friction pair exhibit high surface roughness due to material deformation and interlocking caused

by normal load, as well as debris resulting from adhesion and material removal caused by shear force. The result of Ref. [10] revealed that the low plastic shear resistance is a reason for the large amount of wear of titanium alloys. These factors ultimately lead to a deep plow-cutting feature on their surfaces [39], so that both the substrate and friction pair demonstrate adhesive and abrasive wear mechanisms, where the combined effect of adhesion and abrasion results in significant wear. As another aspect, the strong adhesion between titanium alloys makes it have a large friction coefficient.

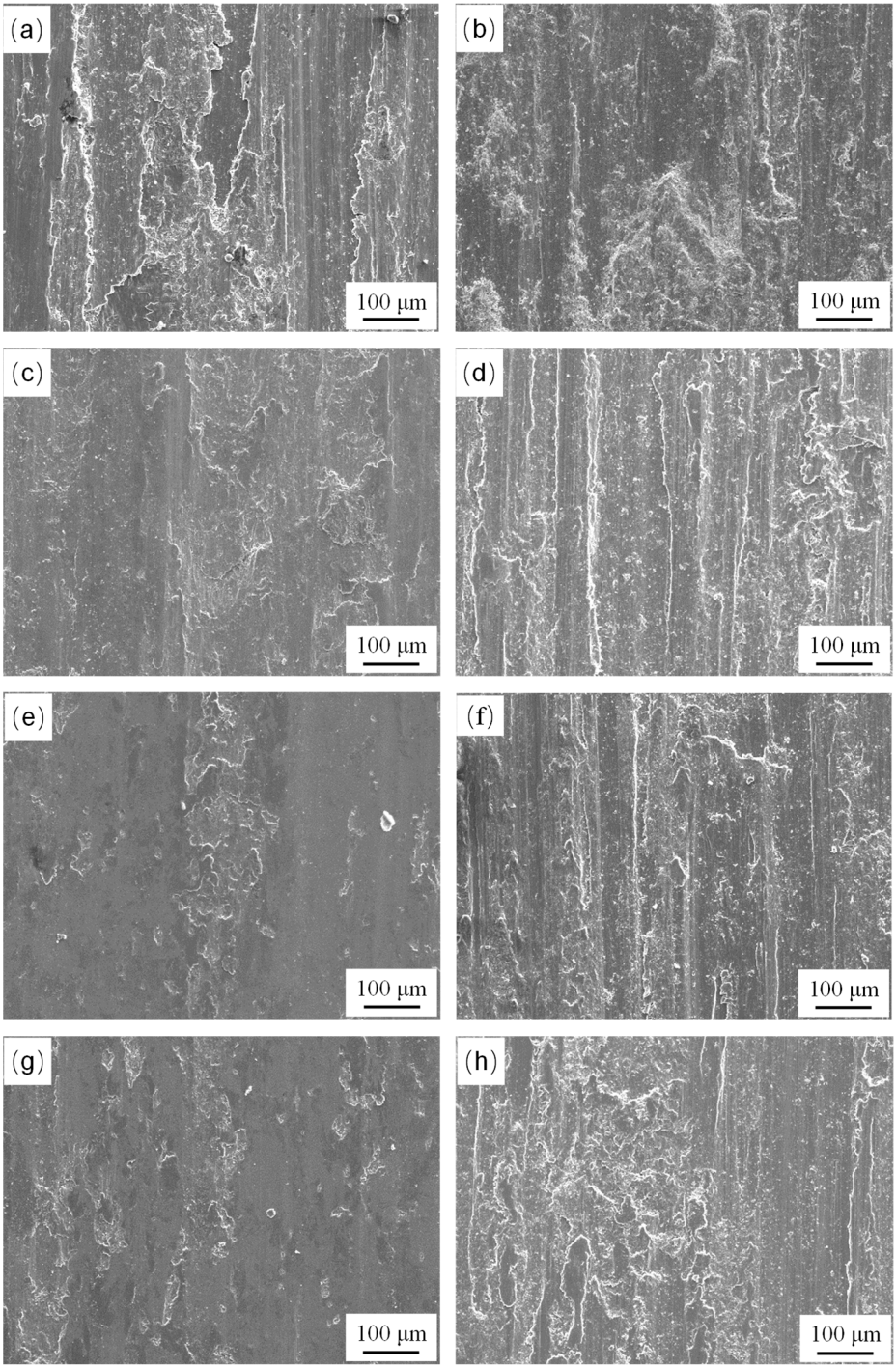


Figure 13. Wear morphology of coatings and friction pair: (**a**) Ti6Al4Vand (**b**) Ti6Al4V friction pair; (**c**) Ni40 coating and (**d**) Ti6Al4V friction pair; (**e**) Ni50 coating and (**f**) Ti6Al4V friction pair; (**g**) Ni60 coating and (**h**) Ti6Al4V friction pair.

Figure 13c,d illustrate the wear trace morphology of the Ni40 coating and the Ti6Al4V friction pair, respectively. The wear trace surface of the Ni40 coating displays flake-like features and "pits" attributed to fatigue and delamination of the coating surface. The surface roughness of the wear trace is notably lower than that observed on the Ti6Al4V substrate, aligning with the results in Figure 10. Owing to its higher hardness relative to the Ti6Al4V substrate, contact deformation of the Ni40 coating is minimized during friction with a Ti6Al4V friction pair. Furthermore, it exhibits a lower friction coefficient compared to that of the Ti6Al4V alloy. These factors collectively contribute to reducing adhesion and fatigue effects between the substrate and friction pair, ultimately mitigating substrate wear loss. The amount and roughness of wear on the Ti6Al4V friction pair is diminished because of decreased production of wear particles resulting from reduced adhesion and fatigue effects.

Figure 13e,f depict the wear trace morphology of the Ni50 coating and the Ti6Al4V friction pair, respectively. The wear trace morphology of the Ni50 coating reveals localized fatigue delamination features linearly distributed along the friction direction, with a smaller area of delamination compared to Ni40 coatings. In addition to spalling features, the remaining worn surfaces exhibit weak cutting characteristics caused by abrasive particles. Similarly, the wear trace of the Ti6Al4V friction pair also displays furrow cutting characteristics caused by abrasive particles when compared to the Ti6Al4V friction pair in contact with both the Ti6Al4V substrate and Ni40 coating. Furthermore, there has been a further reduction in the coefficient of friction, resulting in a decreased adhesion effect between the coating and friction pair, thereby reducing the wear loss and surface roughness of the wear trace.

Figure 13g,h depict the wear trace morphology of the Ni60 coating and the Ti6Al4V friction pair, respectively. The wear trace morphology of the Ni60 coating exhibits similar delamination features to those observed in the Ni50 coating. The fatigue delamination features of NiCrBSi coatings are also observed in ref [40]. NiCrBSi coatings exhibit superior hardness compared to Ti6Al4V and demonstrate resistance to plastic deformation or plowing during friction [32,41], resulting in exceptional wear resistance when compared to Ti6Al4V. As depicted in Figure 13h, the Ti6Al4V friction pair exhibits a rough surface with significant furrow cutting marks compared to the Ni50 coating friction pair. The wear trace roughness results shown in Figure 10 also indicate the higher surface roughness of the Ti6Al4V friction pair. Micrographs in Figures 5 and 6 reveal that the Ni50 coating contains hard phase particles ranging from 10 to 50 μm, while the Ni60 coating contains larger hard phase particles ranging from 25 to 100 μm. The more pronounced cutting effect of the hard phase in the Ni60 coating leads to an increase in abrasive particles produced by the TC4 friction pair, intensifying its cutting effect on both the coating and Ti6Al4V friction pair, ultimately resulting in increased wear loss and surface roughness for both components. There are more large granular hard phases in Ni60 coatings than in Ni50 coatings. Throughout the wear process of Ni60, there is a continuous shedding of hard phases that actively participate in wear [42], thereby exacerbating both the wear of the coating and Ti6A4V alloy.

Figure 14 depicts the distribution of the Ti element on the wear trace surface of the coatings analyzed by energy-dispersive spectroscopy (EDS) during scanning electron microscope (SEM) analysis. In Figure 14a, it is evident that the wear trace surface of the Ni40 coating exhibits substantial adhesion of wear debris, indicating a relatively high content of Ti elements. This suggests that the Ti peeled off from the friction pair during the friction process and adhered to the coating surface as abrasive particles. The distribution of the Ti element in Figure 14b is more uniform, with significantly lower characteristic X-ray intensity compared to the Ni40 coating. The presence of Ti as wear debris rather than abrasive particles indicates a weakened adhesion effect between the Ni50 coating and the Ti6Al4V. Furthermore, in Figure 13c, it is apparent that the adhesion effect between the Ni60 coating and Ti6Al4V is further weakened, with uniform distribution of the Ti element as wear debris on the wear trace. It becomes clear that an increase in coating hardness leads to

decreased adhesion between the coating and Ti6Al4V friction pair, resulting in a reduction in the friction coefficient for these coatings. Compared to Ni40 coatings with relatively low hardness which exhibit a mixed wear mechanism consisting mainly of adhesion wear and fatigue wear resulting from adhesion, Ni50 and Ni60 coatings with relatively high hardness show dominant wear mechanisms characterized by fatigue and abrasive wear. The production of abrasive particles in the Ni50 coating due to coating fatigue spalling and the cutting effect on the friction pair by the hard phase is less than those in the Ni40 and Ni60 coatings, respectively, explaining why both have higher levels of abrasion compared to their counterparts.

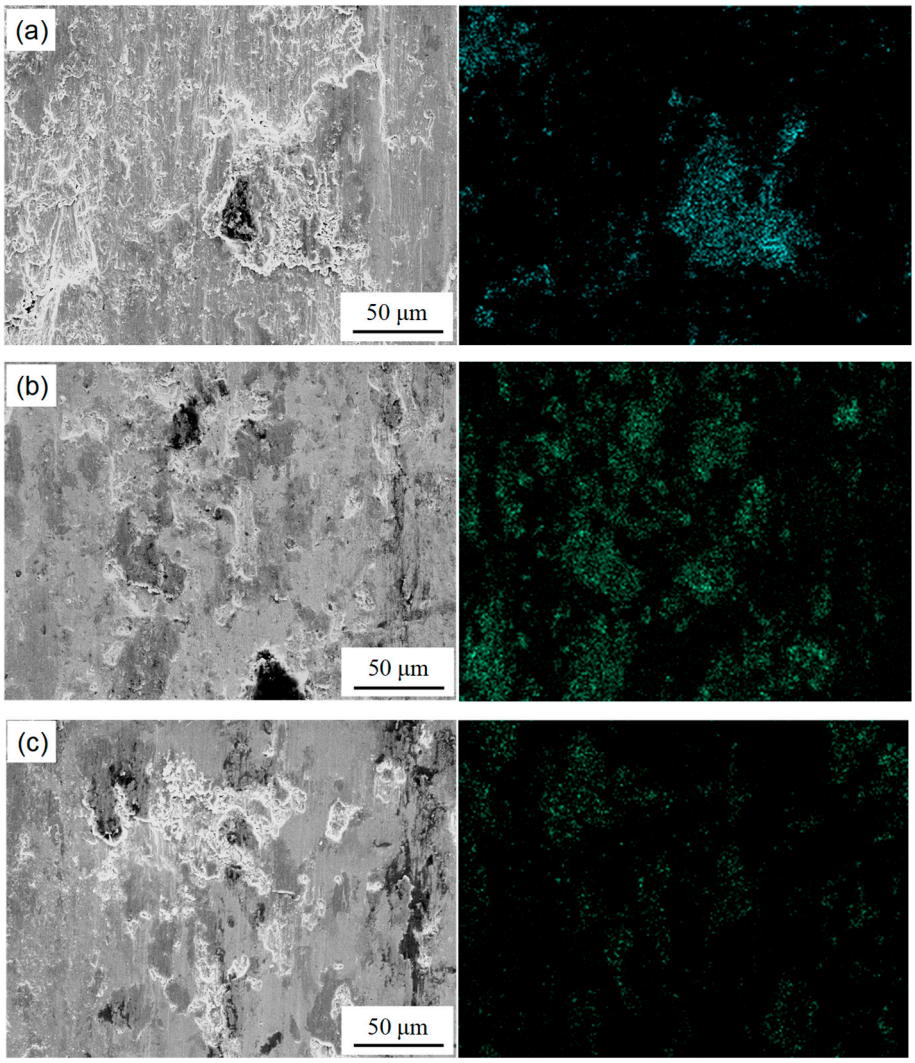


Figure 14. Ti element distribution on wear trace surface of coating: (**a**) Ni40; (**b**) Ni50; (**c**) Ni60.

4. Conclusions

NiCrBSi coatings with different element contents were deposited on the surface of the Ti6Al4V alloy using the laser cladding process. The mechanical properties of the coatings and the tribological properties of the NiCrBSi coatings in friction with the Ti6Al4V friction pair were analyzed and tested. The conclusions are as follows:

(1) With an increased amount of C and Cr, more and larger hard phases are produced, resulting in an increase in coating hardness. The hardness of the laser-clad Ni40, Ni50, and Ni60 coatings increases gradually.

(2) The NiCrBSi coating reduces the friction coefficient of the Ti6Al4V substrate when in friction with a Ti6Al4V friction pair. The friction coefficient decreases gradually

with an increase in coating hardness, indicating the good lubricating effect of the NiCrBSi coatings.

(3) The Ni50 coating with a hardness of 609 $HV_{0.3}$ shows a minimum specific wear rate compared to that of the Ni40 and Ni60 coatings; it is only 8.4%, 35.4%, and 36.9% that of the Ti6Al4V substrate, Ni40 coating, and N60 coating, respectively. Meanwhile, the wear loss for Ti6Al4V friction pairs in friction with a Ni50 coating is only 36.4%, 52.5%, and 55.3% of that in friction with the Ti6A14V substrate, Ni40 coating, and Ni60 coating, respectively.

(4) Preparing the Ni50 coating on the surface of non-load-bearing titanium alloy parts can reduce the abrasion between titanium alloy parts that is caused by sliding, which is a vital choice for improving the reliability of load-bearing and non-load-bearing titanium alloy parts.

Author Contributions: Writing—original draft preparation, M.F.; writing—review and editing, P.D.; validation, K.W.; data curation, R.Z.; methodology, S.Y.; project administration and conceptualization, T.C. All authors have read and agreed to the published version of the manuscript.

Funding: This research received no external funding.

Institutional Review Board Statement: Not applicable.

Informed Consent Statement: Informed consent was obtained from all subjects involved in this study.

Data Availability Statement: All data that support the findings of this study are included within the article.

Conflicts of Interest: Author M.F. was employed by the China Academy of Machinery Wuhan Research Institute of Materials Protection Co., Ltd.. The remaining authors declare that the research was conducted in the absence of any commercial or financial relationships that could be construed as a potential conflict of interest.

References

1. Singh, P.; Pungotra, H.; Kalsi, N.S. On the characteristics of titanium alloys for the aircraft applications. *Mater. Today Proc.* **2017**, *4*, 8971–8982. [CrossRef]
2. Christoph, L.; Frank, K.; Joachim, H.; Wolfgang, A.K. Materials and design concepts for high performance compressor components. *Aerosp. Sci. Technol.* **2003**, *7*, 201–210.
3. Tan, L.J.; Yao, Z.K.; Zhou, W.; Guo, H.Z.; Zhao, Y. Microstructure and properties of electron beam welded joint of Ti–22Al–25Nb/TC11. *Aerosp. Sci. Technol.* **2010**, *14*, 302–306. [CrossRef]
4. Ning, Y.Q.; Xie, B.C.; Fu, M.W.; Liang, H.Q.; Yao, Z.K.; Guo, H.Z. Microstructure and superplastic deformation for aerospace Ti-alloys associated with α -phase curing behavior. *Aerosp. Sci. Technol.* **2015**, *45*, 416–421. [CrossRef]
5. Mukund, D.S.; Rakesh, S. Dry sliding friction and wear behavior of titanium alloy (Ti-6Al-4V). *Tribol. Online* **2012**, *7*, 87–95.
6. Chauhan, S.R.; Dass, K. Dry sliding wear behaviour of titanium (grade 5) alloy by using response surface methodology. *Adv. Tribol.* **2013**, *1*, 272106. [CrossRef]
7. Łępicka, M.; Grądzka-Dahlke, M. Surface modification of Ti6Al4V titanium alloy for biomedical applications and its effect on tribological performance-a review. *Rev. Adv. Mater. Sci.* **2016**, *46*, 86–103.
8. Molinari, A.; Straffelini, G.; Tesi, B.; Bacci, T. Dry sliding wear mechanisms of the Ti6Al4V alloy. *Wear* **1997**, *208*, 105–112. [CrossRef]
9. Fan, W.T.; Chen, H.J.; Liu, D.F. Effect of Mo on microstructures and wear properties of in situ synthesized Ti(C,N)/Ni-based composite coatings by laser cladding. *Materials* **2017**, *10*, 1047. [CrossRef]
10. Guo, J.; Yan, H.; Zhang, P. Laser cladding NiCrBSi/TiN/h-BN self-lubricating wear resistant coating on Ti-6Al-4V surface. *Mater. Res. Express* **2019**, *6*, 066537. [CrossRef]
11. Fan, X.H.; Geng, L.; Xu, B.; Li, J. Laser cladding NiCrBSi+ 2% B4C coating on Ti-6Al-4V. *Adv. Mater. Res.* **2009**, *4*, 473–476. [CrossRef]
12. Jegadeeswaran, N.; Ramesh, M.; Bhat, U.K. Oxidation resistance HVOF sprayed coating 25% (Cr_3C_2-25(Ni20Cr)) + 75%NiCrAlY on titanium alloy. *Procedia Mater. Sci.* **2014**, *5*, 11–20. [CrossRef]
13. Hua, S.W.; Pang, M.; Chen, J.; Ji, F.Q. Effects of frictional loading on tribological properties of laser cladding Ti2AlC/TC4-Coated TiC particle-reinforced coatings on Ti6Al4V. *J. Mater. Eng. Perform.* **2024**, *33*, 2077–2092. [CrossRef]
14. He, B.F.; Ma, F.; Ma, D.Y.; Xu, K.W. Study of Microstructure and properties of laser cladding Ni60-WC+ TiC composite coating. *Sci. Adv. Mater.* **2020**, *12*, 659–664. [CrossRef]

15. Ma, A.; Liu, D.; Zhang, X.; He, G.; Liu, D.; Liu, C.; Xu, X. The fretting fatigue performance of Ti-6Al-4V alloy influenced by microstructure of CuNiIn coating prepared via thermal spraying. *Tribol. Int.* **2020**, *145*, 106156. [CrossRef]
16. Niu, Z.Q.; Zhou, W.L.; Wang, C.L.; Cao, Z.W.; Yang, Q.; Fu, X.S. Fretting wear mechanism of plasma-sprayed CuNiIn coating on Ti-6Al-4V substrate under plane/plane contact. *Surf. Coat. Technol.* **2021**, *408*, 126794. [CrossRef]
17. Costa, M.Y.; Venditti, M.L.; Voorwald, H.J.; Cioffi, M.O.; Cruz, T.G. Effect of WC-10% Co-4% Cr coating on the Ti-6Al-4V alloy fatigue strength. *Mater. Sci. Eng. A* **2009**, *507*, 29–36. [CrossRef]
18. Mary, C.; Fouvry, S.; Martin, J.M.; Bonnet, B. Pressure and temperature effects on Fretting Wear damage of a Cu-Ni-In plasma coating versus Ti17 titanium alloy contact. *Wear* **2011**, *272*, 18–37. [CrossRef]
19. Du, P.C.; Liu, C.; Hu, H.; Zhang, C.; Fan, M.; Gao, M.; Chen, T. Study of the tribological properties of HVOF-sprayed Ni-based coatings on Ti6Al4V titanium alloys. *Coatings* **2022**, *12*, 1977. [CrossRef]
20. Liu, X.B.; Liu, H.Q.; Liu, Y.F.; He, X.M.; Sun, C.F.; Wang, M.D.; Yang, H.B.; Qi, L.H. Effects of temperature and normal load on tribological behavior of nickel-based high temperature self-lubricating wear-resistant composite coating. *Compos. Part B Eng.* **2013**, *53*, 347–354. [CrossRef]
21. Somervuori, M.; Varis, T.; Oksa, M.; Suhonen, T.; Vuoristo, P. Comparative study on the corrosion performance of APS-, HVOF-, and HVAF-sprayed NiCr and NiCrBSi coatings in NaCl solutions. *J. Therm. Spray Technol.* **2022**, *31*, 1581–1597. [CrossRef]
22. Liu, K.; Yan, H.; Zhang, P.; Zhao, J.; Yu, Z.; Lu, Q. Wear behaviors of TiN/WS_2+ hBN/NiCrBSi self-lubricating composite coatings on TC4 alloy by laser cladding. *Coatings* **2020**, *10*, 747. [CrossRef]
23. Sun, R.L.; Yang, D.Z.; Guo, L.X.; Dong, S.L. Microstructure and wear resistance of NiCrBSi laser clad layer on titanium alloy substrate. *Surf. Coat. Technol.* **2000**, *132*, 251–255. [CrossRef]
24. Li, W.G.; Li, J.; Xu, Y.S. Optimization of corrosion wear resistance of the NiCrBSi laser-clad coatings fabricated on Ti6Al4V. *Coatings* **2021**, *11*, 960. [CrossRef]
25. Luo, X.; Li, J.; Li, G.J. Effect of NiCrBSi content on microstructural evolution, cracking susceptibility and wear behaviors of laser cladding WC/Ni–NiCrBSi composite coatings. *J. Alloys Compd.* **2015**, *626*, 102–111. [CrossRef]
26. Liu, R.X.; Lei, T.Q.; Guo, L.X. Stratification mechanism and interface characterization of (TiN), (TiC)/NiCrBSi composite coatings synthesized by laser remelting. *Surf. Rev. Lett.* **2004**, *11*, 291–295. [CrossRef]
27. Sun, R.L.; Lei, Y.W.; Niu, W. Laser clad TiC reinforced NiCrBSi composite coatings on Ti-6Al-4V alloy using a CW CO_2 laser. *Surf. Coat. Technol.* **2009**, *203*, 1395–1399. [CrossRef]
28. Gao, Q.S.; Yan, H.; Qin, Y.; Zhang, P.L.; Gao, J.L.; Chen, Z.F.; Yu, Z.S. Laser cladding Ti-Ni/TiN/TiW+TiS/WS_2 self-lubricating wear resistant composite coating on Ti-6Al-4V alloy. *Opt. Laser Technol.* **2019**, *113*, 182–191. [CrossRef]
29. Conde, A.; Zubiri, F. Cladding of Ni-Cr-B-Si coatings with a high power diode laser. *Mater. Sci. Eng. A* **2002**, *334*, 233–238. [CrossRef]
30. Fernández, E.; Cadenas, M.; González, R.; Navas, C.; Fernández, R.; De Damborenea, J. Wear behaviour of laser clad NiCrBSi coating. *Wear* **2005**, *259*, 870–875. [CrossRef]
31. Li, G.L.; Li, Y.L.; Dong, T.S.; Wang, H.D.; Zheng, X.D.; Zhou, X.K. Microstructure and wear resistance of TIG remelted NiCrBSi thick coatings. *Adv. Mater. Sci. Eng.* **2018**, *2018*, 1–10. [CrossRef]
32. Zhang, D.W.; Lei, T.C.; Li, F.J. Laser cladding of stainless steel with Ni–Cr_3C_2 for improved wear performance. *Wear* **2001**, *251*, 1372–1376. [CrossRef]
33. Houdková, Š.; Smazalová, E.; Vostřák, M.; Schubert, J. Properties of NiCrBSi coating, as sprayed and remelted by different technologies. *Surf. Coat. Technol.* **2014**, *253*, 14–26. [CrossRef]
34. Otsubo, F.; Era, H.; Kishitake, K. Structure and phases in nickel-base self-fluxing alloy coating containing high chromium and boron. *J. Therm. Spray Technol.* **2000**, *9*, 107–113. [CrossRef]
35. Liu, X.Y. Heterogeneous nucleation or homogeneous nucleation. *J. Chem. Phys.* **2000**, *112*, 9949–9955. [CrossRef]
36. Kao, W.H.; Su, Y.L.; Horng, J.H.; Huang, H.C. The tribological performance of surface treated Ti6A14V as sliding against Si_3N_4 ball and 316L stainless steel cylinder. *J. Mater. Eng. Perform.* **2016**, *25*, 5209–5219. [CrossRef]
37. Budinski, K.G. Tribological properties of titanium alloys. *Wear* **1991**, *151*, 203–217. [CrossRef]
38. Dong, H. Tribological properties of titanium-based alloys. *Surf. Eng. Light Alloys* **2010**, 58–80. [CrossRef]
39. Magaziner, R.S.; Jain, V.K.; Mall, S. Investigation into wear of Ti-6Al-4V under reciprocating sliding conditions. *Wear* **2009**, *267*, 368–373. [CrossRef]
40. Bin, C.; Tan, Y.F.; Tu, Y.Q.; Wang, X.L.; Hua, T.A. Tribological properties of Ni-base alloy composite coating modified by both graphite and TiC particles. *Trans. Nonferrous Met. Soc. China* **2011**, *21*, 2426–2432.
41. Yan, H.; Zhang, P.; Yu, Z.; Lu, Q.; Yang, S.; Li, C. Microstructure and tribological properties of laser-clad Ni–Cr/TiB_2 composite coatings on copper with the addition of CaF_2. *Surf. Coat. Technol.* **2012**, *206*, 4046–4053. [CrossRef]
42. Wang, H.; Xia, W.M.; Jin, Y.S. A study on abrasive resistance of Ni-based coatings with a WC hard phase. *Wear* **1996**, *195*, 47–52. [CrossRef]

Disclaimer/Publisher's Note: The statements, opinions and data contained in all publications are solely those of the individual author(s) and contributor(s) and not of MDPI and/or the editor(s). MDPI and/or the editor(s) disclaim responsibility for any injury to people or property resulting from any ideas, methods, instructions or products referred to in the content.